

Resonant Tunneling and Intrinsic Bistability in Twisted Graphene Structures

J. F. Rodriguez-Nieva¹, M. S. Dresselhaus^{1,2}, L. S. Levitov¹

¹*Department of Physics, Massachusetts Institute of Technology, Cambridge, MA 02139, USA and*

²*Department of Electrical Engineering and Computer Science, Massachusetts Institute of Technology, Cambridge, MA 02139, USA*

We propose a novel mechanism for intrinsic bistability in van der Waals heterostructures formed by multiple twisted graphene layers. Bistability in these systems originates from resonant tunneling and charge coupling between different graphene layers. These characteristics, governed by the Dirac-like spectrum and Moiré periodicity of the tunneling Hamiltonian, allow multiple stable states in the sequential tunneling regime. In the bistability region, an intermediate electrically decoupled graphene layer can, for the same external bias, be either in a resonant or non-resonant state with respect to the top/bottom layer. Features of interest, such as resonant tunneling, negative differential resistance and bistability, are controlled by *geometric* device parameters easily accessible in experiments, namely the twist angle and the interlayer distances.

Bistable systems exhibit several distinct macroscopic states and can switch between them upon variation of some control parameter. Volatile and non-volatile electronic systems that exhibit intrinsic bistability and fast switching times are desirable for low-power memory and logic [1]. Experimental realizations of such systems, however, are scarce (e.g. [2–9]). Van der Waals heterostructures afford new ways of designing novel electronic environments with tailored band structures and transport characteristics [10]. Their large degree of tunability and compactness allows to envision a new class of electronically bistable systems that exploit the unique characteristics of novel 2D materials. Here we propose one such way to obtain intrinsically bistable I - V characteristics using van der Waals heterostructures formed by twisted graphene monolayers.

Bistability in these systems originates from resonant tunneling between twisted graphene monolayers in the sequential tunneling regime [Fig.1(a)]. In particular, resonances in the tunneling current rely on the characteristics of the Dirac-like spectrum of twisted graphene monolayers [see Fig.1(b)] and the Moiré periodicity of the tunneling Hamiltonian [11]. The origin of these resonances can be most readily understood as the consequence of the alignment of the ‘twisted’ Dirac cones by the action of an electrostatic potential build-up between layers, as shown in Fig.1(c) [12]. Because of the non-monotonic I - V characteristics, multiple stable configurations of an electrically decoupled graphene layer [middle layer in Fig.1(a)] are possible in the sequential tunneling regime. As shown in Fig.1(c), in the bistability region this decoupled layer can, for the same external bias, be either in a resonant (low resistance) or non-resonant (high-resistance) state with respect to the other layers.

A particularly appealing feature of bistability in graphene heterostructures is that the I - V characteristics are mainly controlled by a few parameters which are easily accessible in experiments, namely the twist angle θ and the interlayer distances between layers, d_{12} and d_{23} in Fig.1(a). This allows a unique *geometrical* control of

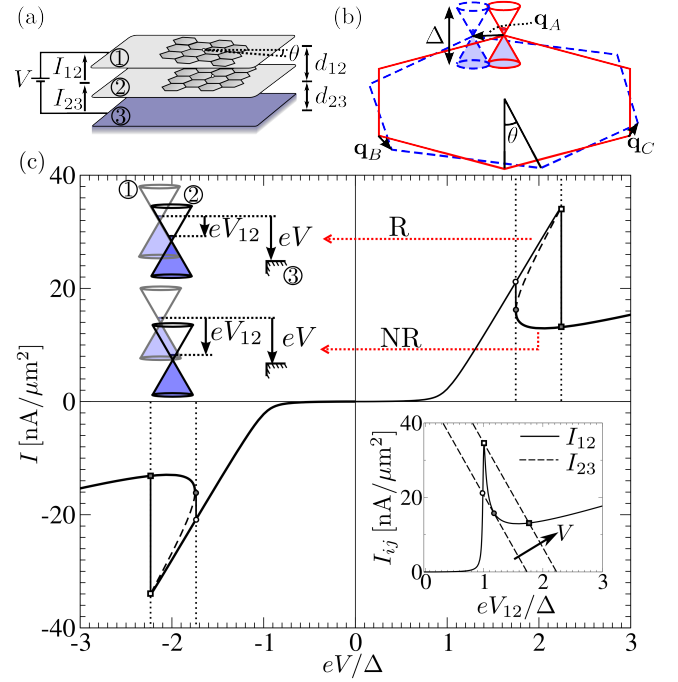


FIG. 1. Intrinsically bistable I - V characteristics in twisted graphene devices. Shown are (a) device schematics, (b) twisted bilayer band-structure and (c) bistable I - V characteristics. Here layers are labelled 1 to 3 from top to bottom, θ is the angle of rotation between the top and middle graphene lattices thus defining an energy scale Δ [Eq.(1)], $\mathbf{q}_{A,B,C}$ are the superlattice wavevectors [Eq.(4)], I_{ij} , V_{ij} and d_{ij} are the current, voltage, and interlayer distances between layers i and j , respectively. The resonant (R) and non-resonant (NR) bistable states, displayed in the upper-left inset of (c), are obtained by solving Eq.(7) [see lower-right inset of (c)].

the I - V response. Indeed, transport and special features of interest, such as the size of the bistability region, can be expressed in terms of two main parameters: a characteristic energy Δ induced by the twisted superlattice, and the interlayer conductance ratio $Z = G_{12}/G_{23}$, with G_{ij} the conductance between layers i and j in Fig.1(a).

These two parameters depend on θ , d_{12} and d_{23} as

$$\Delta = \frac{8\pi\hbar v_F}{3a_0} \sin(\theta/2), \quad Z = \exp[2(d_{23} - d_{12})/\lambda]. \quad (1)$$

Here $v_F \approx 10^6$ m/s is the Fermi velocity, $a_0 \approx 2.46$ Å is the graphene lattice parameter, and λ is the characteristic WKB decay length induced by the interlayer barrier potential (discussed in more detail below).

Importantly, the values of Δ and Z can be controlled in experiments with a large degree of precision. For instance, the twist angle θ can be tuned to within $\sim 1^\circ$ during fabrication [12]. Furthermore, control of Z is achieved by adding monolayers of dielectric materials, such as hBN or MoS₂. Because typical values of $\lambda = \hbar/\sqrt{2m_e W} \sim 2$ Å are comparable to the thickness of a single layer of dielectric material, adding single layers of dielectric materials allows a sufficiently slow variation of Z with d_{ij} (here we used a typical barrier height $W \sim 1$ eV and an effective electron mass in barrier region $m_e \sim 9 \cdot 10^{-31}$ kg).

In addition to the large degree of tunability, the graphene heterostructure approach features other exceptional properties. Because of the small interlayer transport lengths, these devices would allow high operation speeds and fast-switching times. Further, the atomically thin nature that is characteristic of van der Waals heterostructures makes it possible to achieve large packing densities. These features are not all present in more traditional approaches toward achieving bistability in graphene-based systems, such as in graphene flash memories [5, 6] or graphene resistive memories [7–9].

Turning to the details of the model, we consider here a system formed by three layers, labelled 1-3 in Fig.1(a). The middle graphene layer (layer 2) is electrically decoupled, whereas the top and bottom layers are contacted with external electron reservoirs. We assume that the contact resistance is sufficiently small so that all the potential drop occurs between layers. When the interlayer coupling is sufficiently small such that tunneling times are smaller than electron relaxation times, transport occurs sequentially between layers.

Coherent transport between a pair of twisted graphene layers is mainly governed by θ . The value of θ determines the (minimum) wavevector \mathbf{q} that can be transferred by the superlattice potential, which is given by $|\mathbf{q}| = \Delta/\hbar v_F = (8\pi/3a_0)\sin(\theta/2)$ [see Fig.1(b)]. Although shorter wavelength Fourier components of the interlayer hopping potential also contribute to tunneling, it has been shown that they fall to zero very rapidly on the reciprocal lattice vector scale [13, 14]. This value of $|\mathbf{q}|$ defines the separation between Dirac cones in reciprocal space of the twisted layers, and determines the characteristic interlayer electrostatic potential necessary for resonances in the tunneling current to occur. If $|\mathbf{q}|$ is too large, transport cannot occur coherently and second order processes dominate.

In our sequential tunneling model, we consider that the first step in the tunneling process occurs coherently between layers 1 and 2. To simplify the discussion without changing the essence of bistability, the second step (between 2 and 3) is assumed to occur incoherently and is described by Ohm's law. This is the case when layer 3 is a graphene layer with a large twist angle with respect to the middle layer, but can also be the case if layer 3 is made of a different material so that there is a large mismatch between unit cells of layer 2 and 3.

The low energy Hamiltonian describing coherent transport between two graphene layers is $\mathcal{H} = \mathcal{H}_0 + \mathcal{T}$, where \mathcal{H}_0 is the free-particle kinetic term describing massless Dirac particles in both graphene layers, and \mathcal{T} describes the coupling between layers [13–15]. The free particle component \mathcal{H}_0 is given by

$$\mathcal{H}_0 = \sum_{i=1,2} \sum_{\mathbf{k}} \psi_{i,\mathbf{k}}^\dagger [\hbar v_F (\boldsymbol{\sigma}_i \cdot \mathbf{k}) - e\Phi_i] \psi_{i,\mathbf{k}}. \quad (2)$$

Here $i = 1, 2$ labels the graphene layer, Φ_i is the electrostatic potential of layer i (which shifts the energy spectrum with respect to the ground state value), $\boldsymbol{\sigma}_i = e^{i\sigma_z \theta_i/2} \boldsymbol{\sigma} e^{-i\sigma_z \theta_i/2}$ are rotated Pauli matrices, and θ_i is the angle of layer i with respect to a fixed coordinate system. Hereafter we use $\theta = \theta_2 - \theta_1$. For a small twist angle θ , the intervalley coupling can be ignored and thus, it is not necessary to describe both valleys in Eq.(2).

The tunneling Hamiltonian can be assumed as a local, periodic and slowly varying function of position [13] described by

$$\mathcal{T} = \sum_{j=A,B,C} \sum_{\mathbf{k}} \psi_{1,\mathbf{k}}^\dagger [t_\perp \mathbf{T}^{(j)}] \psi_{2,\mathbf{k}+\mathbf{q}_j} + \text{c.c.} \quad (3)$$

Here the coefficient t_\perp is the interlayer hopping amplitude, and $j = A, B, C$ labels the three dominant momentum transfers \mathbf{q}_j [see Fig.1(b)] and the phase matrices $\mathbf{T}^{(j)}$ given by

$$\mathbf{q}_j = \frac{\Delta}{\hbar v_F} (\sin \varphi_j, -\cos \varphi_j), \quad \mathbf{T}^{(j)} = \begin{pmatrix} e^{i\varphi_j} & 1 \\ e^{-i\varphi_j} & e^{i\varphi_j} \end{pmatrix}, \quad (4)$$

with $\varphi_A = 0$, $\varphi_B = 2\pi/3$, $\varphi_C = 4\pi/3$. The tunneling coupling in Eq.(3) is obtained assuming that the top and bottom graphene lattices have a common lattice point [13]. A rigid horizontal translation between lattices adds an additional overall phase to the matrix $\mathbf{T}^{(j)}$ [14]. However, such a phase does not play an important role in bistability, and we set it equal to zero for simplicity. Equations (2) and (3) are expected to be accurate for twist angles $\theta \lesssim 10^\circ$, and energies of 1 eV [15].

As a side remark, we note that the lattice of the dielectric material separating the graphene layers, used here for tuning the interlayer hopping amplitude, can also modulate the slowly varying and periodic tunneling potential if it closely matches the graphene lattice (a detailed discussion can be found in Ref.[16]). This condition may

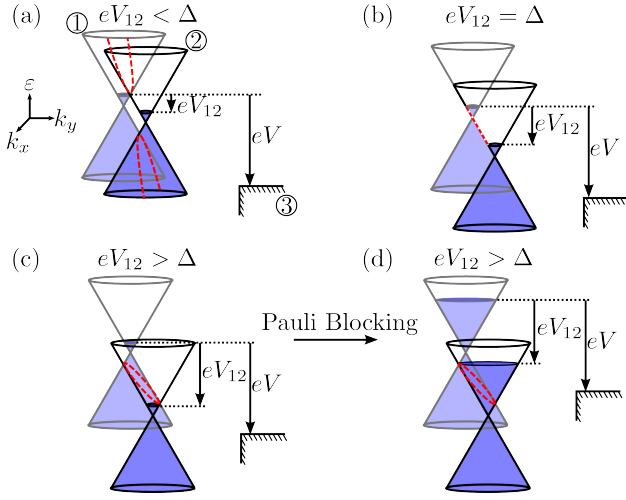


FIG. 2. The regions in phase space of electronic states contributing to the resonant tunneling current (dashed red lines) for a fixed value of V . These regions form conicals in \mathbf{k} -space when the interlayer bias potential between twisted bilayers, V_{12} , takes values $eV_{12} < \Delta$ (hyperbolic curve) and $eV_{12} > \Delta$ (ellipsoidal curve). When $eV_{12} = \Delta$, a van-Hove singularity in the tunneling density of states is obtained, thus allowing a resonant (low resistance) bistable state. Interestingly, the non-resonant (high-resistance) bistable state ($eV_{12} > \Delta$) can be Pauli-blocked with doping, as shown in (d). Thus, doping affords a way to tune the current ratio between bistable branches in Fig.1(a). Here, it is assumed that the Dirac cones are aligned at $V = 0$ and capacitance effects are neglected. Layers are labelled 1-3 as in Fig.1(a).

be relevant, for instance, in the case of hBN (1.8% lattice mismatch) when the hBN lattice is oriented with the graphene lattice. The values of \mathbf{q}_j can then be modified from those defined above, but this does not affect the bistability physics that we describe and is thus not considered here explicitly.

The tunneling current I_{12} between layers 1 and 2 under a bias potential is given by

$$I_{12} = \frac{eD_s D_v |t_\perp|^2}{\hbar} \sum_{\mathbf{k} s s' j} |F_{ss'}^{(j)}(\mathbf{k})|^2 \int_{-\infty}^{\infty} \frac{d\omega}{2\pi} A_{1,s}(\mathbf{k}, \omega) \times A_{2,s'}(\mathbf{k} + \mathbf{q}_j, \tilde{\omega}) [f_1(\omega) - f_2(\tilde{\omega})], \quad (5)$$

where, due to the built-in interlayer electrostatic potential Φ_i [see Eq.(2)], the energy for the quantities in layer 2 is offset by $\tilde{\omega} = \omega + e(\Phi_2 - \Phi_1)$. In Eq.(5), s (s') refers to the electron (+) and hole (-) bands of layer 1 (2), D_s (D_v) is the spin (valley) degeneracy, $A_{i,s}$ is the spectral function of layer i and band s , $f_i(\omega) = 1/[e^{\beta(\omega - \mu_i)} + 1]$ is the Fermi distribution function of layer i , with $\beta = 1/k_B T$ the inverse thermal energy and μ_i is the Fermi energy of layer i . The phase factor $F_{ss'}^{(j)}$ in Eq.(5) is calculated as

$$F_{ss'}^{(j)}(\mathbf{k}) = u_{1,s}^\dagger(\mathbf{k}) \mathbf{T}^{(j)} u_{2,s'}(\mathbf{k} + \mathbf{q}_j), \quad (6)$$

where $u_{i,s}^\dagger(\mathbf{k}) = \sqrt{1/2}[1, se^{-i(\theta_{\mathbf{k}} - \theta_i)}]$ is the two-component eigenvectors of Eq.(2) with eigenvalues $\varepsilon_{i,s}(\mathbf{k}) = s\hbar v_F |\mathbf{k}| + e\Phi_i$ and $\theta_{\mathbf{k}}$ is the polar angle of the \mathbf{k} vector. Transport between layers 2 and 3 is assumed to occur incoherently and is described by Ohm's law $I_{23} = G_{23} \cdot V_{23}$, where G_{23} is the interlayer conductance and V_{23} is the bias potential between layers 2 and 3.

For simplicity, in Eq.(5) we fix the Fermi energies to some constant value, $\mu_{1,2} = \mu$, thus turning off quantum capacitance effects [17]. In this case, the potential difference between layers 1 and 2, V_{12} , is related to the electrostatic potentials Φ_1 and Φ_2 in Eq.(2) as $V_{12} = \Phi_2 - \Phi_1$, like what happens typically in a metal (see Fig.2). This approximation is valid in the regime $4e^2 d_{12} \Delta / \kappa (\hbar v_F)^2 \approx 15 \cdot d_{12} [\text{nm}] \Delta [\text{eV}] / \kappa \gg 1$, with κ the dielectric constant of the barrier material, such that minimal changes in carrier concentration induce large interlayer electrostatic potentials. The more realistic scenario which includes quantum capacitance effects, such that $\mu_{1,2}$ and $\Phi_{1,2}$ are implicit functions of V_{12} , is here considered in the Appendix. However, this more realistic picture only introduces small corrections to the tunneling current, without altering the essence of our bistability discussion in the main text.

The I - V characteristics of the system are determined self-consistently by fixing the total external bias $V = V_{12} + V_{23}$ between the bottom and the top layer. The equilibrium current I at fixed V is then calculated by finding V_{12} from the non-linear equation

$$I(V) = I_{12}(V_{12}) = I_{23}(V - V_{12}). \quad (7)$$

This procedure is shown graphically in the inset of Fig.1(c). Given the non-monotonicity of I_{12} , Eq.(7) allows multiple stable solutions.

In order to assign numerical values to the tunneling current, we assume a twist angle $\theta = 2^\circ$, which defines an energy scale $\Delta = 0.37$ eV. Furthermore, we take a Lorentzian spectral function in Eq.(5) for both layers, $A_{i,s}(\mathbf{k}, \omega) = 2\Gamma / [(\omega - s\hbar v_F |\mathbf{k}|)^2 + \Gamma^2]$, with linewidth $\Gamma \sim 10$ meV. A finite linewidth Γ is necessary to have a finite value of the peak current when $eV_{12} = \Delta$ (see Fig.2). The temperature T of the system was set to $T = 0$, and the Fermi level of all layers was $\mu_i = 0$ for all values of V . With reference to Eq.(5), we define the interlayer conductance

$$G_{12} = S g_{12}, \quad g_{12} = 2\pi D_s D_v \frac{|t_\perp|^2}{(\hbar v_F)^2} \frac{e^2}{h}, \quad (8)$$

where S is the surface area of the device. The value of g_{12} is sensitive to the twist angle and the stacked dielectric material, if any, via the parameter t_\perp . Here we consider $g_{12} = 10^{-7} \Omega^{-1} \mu\text{m}^{-2}$. Similar values of g_{12} were measured in resonant tunneling devices which contained 4 layers of BN in-between the graphenes [11]. For G_{23} , we consider a value of $Z = G_{12}/G_{23} = 0.2$.

The bistable I - V characteristics are shown in Fig.1(c). For a sufficiently high bias, $eV \gtrsim \Delta$, the current branches into two stable states. The upper bistable branch in Fig.1(c) corresponds to two layers in resonance (i.e. $eV_{12} \approx \Delta$, see discussion in Fig.2), while the lower branch corresponds to a non-resonant state (i.e. $eV_{12} > \Delta$). We note that a third solution is also possible, indicated with a dashed line in the I - V response. This solution, however, is unstable given that a small perturbation in the bias δV_{12} will push the system away from this state. For very large biases, $eV \gg \Delta$, the resonant branch becomes unstable. In this case, the current at resonance is not large enough to compensate for an increase in I_{23} .

We show next how the size of the bistability region depends on the model parameters. For this purpose, several simplifications to Eq.(5) can be done. First, we note that the phase factor $F_{ss'}^{(j)}(\mathbf{k})$ varies, upon integration in \mathbf{k} -space, in the range $0 \leq |F_{ss'}^{(j)}(\mathbf{k})| \leq 2$ taking typical values $|F_{ss'}^{(j)}(\mathbf{k})| \approx 1$. Thus, it is a good approximation to take band and wavevector-independent phase factors $|F_{ss'}^{(j)}(\mathbf{k})| = \bar{f}$. Further, in the typical case scenario, we have that $\Gamma (\sim 10 \text{ meV}) \ll \Delta (\sim 0.1 - 1 \text{ eV})$. With this in mind, the integration of Eq.(5) allows an analytical form expressed in terms of line integrals in conical surfaces (see Fig.2 and discussion in Appendix). Using $\mu_{1,2} = 0$ and $V_{12} = \Phi_2 - \Phi_1$, we find that the non-resonant interlayer current takes the simple form

$$\frac{I_{12}(x)}{I_{\min}} = \frac{x^2 - 1/2}{\sqrt{2(x^2 - 1)}}, \quad I_{\min} = \frac{3\sqrt{2}\bar{f} G_{12}\Delta}{4e}, \quad (9)$$

with $x = eV_{12}/\Delta > 1$ and I_{\min} the minimum current obtained at $x_{\min} = \sqrt{3/2}$. When $eV_{12}/\Delta = 1$, the current peaks and reaches a maximum value which is sensitive to Γ . To leading order in Γ , we obtain

$$I_{\max} = I_{12}(\Delta/e) = \pi\sqrt{\Delta/2\Gamma}I_{\min}, \quad (10)$$

where Γ will in general depend on the amount and type of disorder and/or temperature.

As a crude estimate, we can now use the values of I_{\min} and I_{\max} above to calculate the width of the bistability region $V_w \approx (I_{\max} - I_{\min})/G_{23}$, giving $eV_w/\Delta \approx (3\sqrt{2}\bar{f}Z/4) \cdot (\pi\sqrt{\Delta/2\Gamma} - 1)$. Importantly, very small values of Z ($G_{23} \gg G_{12}$) would make the bistability region negligibly small, whereas large values of Z ($G_{23} \ll G_{12}$) would push the onset of the bistability region to very large bias potentials. Optimally, values of $Z \sim 1$ and very small Γ would make the bistability effect more prominent.

As discussed above, the value of Z in Eq.(1) can be controlled with the thicknesses d_{ij} . This can be obtained from the Bardeen Transfer Hamiltonian Theory [18, 19]. In this theory, the interlayer coupling t_{\perp} is calculated from the overlap of the wavefunctions of layers i and j in the barrier region, $t_{\perp} = (\hbar^2/2m_e) \int d\mathbf{S} \cdot$

$(\psi_i^* \nabla \psi_j - \psi_j \nabla \psi_i^*)$, with $d\mathbf{S}$ a surface area element. Taking as approximation electrons tunneling across a square barrier potential of height much larger than the kinetic energy, this model yields a tunneling matrix element $t_{\perp} \propto \exp(-d_{ij}/\lambda)$ governed by the exponential WKB decay length $\lambda = \hbar/\sqrt{2m_e W}$. Assuming barriers between layers 1-2 and 2-3 to be of the same material and using G_{ij} in Eq.(8), then Z in Eq.(1) is obtained.

It is also evident from Eqs.(9) and (10) that the current ratio between bistable branches is controlled by the numerical factor $Z\sqrt{\Delta/\Gamma}$. For realistic values of disorder, this ratio is in the 1-20 ballpark. From the applications point of view, it is interesting to make this current ratio as large as possible. It turns out that in our system this can be achieved by means of Pauli blocking. As shown in Fig.2, for sufficiently heavily doped samples, the non-resonant bistable state (but not the resonant one) can be Pauli blocked, thus leading to very large current ratios between bistable states. How large this ratio is will depend on second order processes which assist tunneling, such as scattering with defects or disorder. These second order processes will not be considered here.

It is interesting to note that the mechanism for bistability described here differs from the one observed in GaAs double-barrier quantum well structures [20]. In the latter case, bistability was explained in terms of the electrostatic feedback produced by the charge of electrons located in the semiconductor quantum well [21]. As such, a bistable ‘charged/uncharged’ quantum well state, accessed by magnetic oscillation measurements [22], is the fingerprint of the double barrier quantum well architecture. The electrostatic feedback mechanism, while also present in our proposed architecture, is not essential for bistability. Indeed, in our discussion above, this mechanism was purposely turned off by making the Fermi energies of all layers constant independently of the bias.

However, we stress that although electrostatic doping of the graphene layers is not essential for the physics that we describe, it is a key feature of bistability. In particular, each bistable state features a different carrier concentration. Thus, any in-plane measurement, such as conductance or magneto-transport, will be able to distinguish two distinct states for a fixed V . From the inset of Fig.1(c), we see that the interlayer bias potential for each bistable state differs by an amount $\delta V_{12} \sim \Delta/e$ (see also discussion in the Appendix). Taking into account the capacitance of the layers, then the induced carrier difference between both states is approximately $\delta n \sim \kappa\Delta/4\pi e^2 d_{12}$ (here the quantum capacitance is not included). Using $\theta = 2^\circ$, $\kappa = 1$ and $d_{12} = 1 \text{ nm}$, we obtain a carrier density difference $\delta n \sim 10^{12} \text{ cm}^{-2}$ between stable states. These large carrier density differentials can be used as a smoking gun of intrinsic bistability.

As a final remark, we note that the main function of the dielectric material stacked between the graphenes is to tune the interlayer coupling and to facilitate the build-up

of the interlayer electrostatic potential in order to achieve a resonant behavior, but is not essential for bistability. Therefore, bistable I - V characteristics may also be possible for twisted graphene trilayers in the absence of any dielectric material. Indeed, incommensurability between graphene lattices already suppresses interlayer hybridization, regardless of being spatially separated by a fraction of a nanometer, thus enabling the experimental realization of the sequential tunneling regime [14]. Furthermore, the Dirac-like spectrum, and thus Eq.(2) and the subsequent transport model, remain valid but with a modified Fermi velocity [13].

In summary, graphene-based van der Waals heterostructures afford a new platform to realize devices with tunable I - V characteristics, including those with intrinsically bistable behavior. The large degree of control of device parameters already achieved experimentally, including twist angle and dielectric thickness, makes our proposal readily accessible to experimentalists. The nanoscale interlayer distance, which results in a fast response and large packing-densities, make these heterostructures appealing for novel memory technologies.

We thank A. D. Liao for useful discussions, and acknowledge financial support from the National Science Foundation Grant DMR1004147.

[1] H.-S. P. Wong and S. Salahuddin, *Nature Nanotechnology* **10**, 191 (2015).
 [2] D. B. Strukov, G. S. Snider, D. R. Stewart and R. S. Williams, *Nature* **453**, 80 (2008).
 [3] J. J. Yang, D. B. Strukov and D. R. Stewart, *Nature Nanotechnology* **8**, 13 (2013).
 [4] A. D. Kent, and D. Worledge, *Nature Nanotechnology* **10**, 187 (2015).
 [5] A. J. Hong, E. B. Song, H. S. Yu, M. J. Allen, J. Kim, J. D. Fowler, J. K. Wassei, Y. Park, Y. Wang, J. Zou, R. B. Kaner, B. H. Weiller, and K. L. Wang, *ACS Nano* **5**, 7812 (2011).
 [6] S. Bertolazzi, D. Krasnozhan, and A. Kis, *ACS Nano* **7**, 3246 (2013).
 [7] Xiaomu Wang, Weiguang Xie, Jun Du, Chengliang Wang, Ni Zhao, and Jian-Bin Xu, *Adv. Mater.* **24**, 2614 (2012).
 [8] Y. J. Shin, J. H. Kwon, G. Kalon, K.-T. Lam, C. S. Bhatia, G. Liang, and H. Yang, *Appl. Phys. Lett.* **97**, 262105 (2010).
 [9] Y. Zheng, G.-X. Ni, C.-T. Toh, M.-G. Zeng, S.-T. Chen, K. Yao, and B. Özyilmaz, *Appl. Phys. Lett.* **94**, 163505 (2009).
 [10] A. K. Geim and I. V. Grigorieva, *Nature* **499**, 419 (2013).
 [11] L. Britnell, R. V. Gorbachev, A. K. Geim, L. A. Ponomarenko, A. Mishchenko, M. T. Greenaway, T. M. Fromhold, K. S. Novoselov, and L. Eaves, *Nature Communications* **4**, 1794 (2013).
 [12] A. Mishchenko, J. S. Tu, Y. Cao, R. V. Gorbachev, J. R. Wallbank, M. T., Greenaway, V. E. Morozov, S. V. Morozov, M. J. Zhu, S. L. Wong, F. Withers, Y.-J. Woods,

C. R. Kim, K. Watanabe, T. Taniguchi, E. E. Vdovin, O. Makarovskiy, T. M. Fromhold, V. I. Fal'ko, A. K. Geim, L. Eaves, and K. S. Novoselov, *Nature Nano* **9**, 808 (2014).
 [13] J. M. B. Lopes dos Santos, N. M. R. Peres, and A. H. Castro Neto, *Phys. Rev. Lett.* **99**, 256802 (2007).
 [14] R. Bistritzer and A. H. MacDonald, *Phys. Rev. B* **81**, 245412 (2010).
 [15] R. Bistritzer and A. H. MacDonald, *PNAS* **108**, 12233 (2011).
 [16] L. Brey, *Phys. Rev. Appl.* **2**, 014003 (2014).
 [17] S. Luryi, *Appl. Phys. Lett.* **52**, 501 (1988).
 [18] J. Bardeen, *Phys. Rev. Lett.* **6**, 57 (1961).
 [19] E. L. Wolf, *Principles of electron tunneling spectroscopy*, Second Edition (Oxford University Press, Oxford, 2012)
 [20] V. J. Goldman, D. C. Tsui, and J. E. Cunningham, *Phys. Rev. Lett.* **58**, 1256 (1987).
 [21] F. W. Sheard and G. A. Toombs, *Appl. Phys. Lett.* **52**, 1228 (1988).
 [22] A. Zaslavsky, V. J. Goldman, D. C. Tsui, and J. E. Cunningham, *Appl. Phys. Lett.* **53**, 1408 (1988).

Analytical Expression for the Vertical Current

We derive here Eqs.(9) and (10) of the main text. Considering that the phase factor $F_{ss'}^{(j)}$ in Eq.(6) takes typical values $|F_{ss'}^{(j)}(\mathbf{k})| \sim 1$, we set $|F_{ss'}^{(j)}(\mathbf{k})| = \bar{f}$, where \bar{f} is a constant independent of the wavevector and band index. Given that generally we have $\Gamma \ll \Delta$, in the case $e\Phi_{12} > \Delta$ we can set $\Gamma \rightarrow 0$ and thus $A_{i,s}(\mathbf{k}, \omega) = 2\pi\delta(\omega - s\hbar v_F|\mathbf{k}|)$. Then, the two delta-functions appearing in Eq.(5) can be absorbed upon integration over ω and \mathbf{k} -space, resulting in a 1D integral along the contour of an ellipse:

$$\sum_{ss'} \int \frac{d\mathbf{k}}{(2\pi)^2} \int_{\omega_1}^{\omega_2} \frac{d\omega}{2\pi} \delta(\omega - s\hbar v_F|\mathbf{k}|) \delta(\tilde{\omega} - s'\hbar v_F|\mathbf{k} + \mathbf{q}|) \\ = \frac{\delta_{s,-}\delta_{s',+}}{16\pi^3(\hbar v_F)^2} \int_{\theta_1}^{\theta_2} d\theta \frac{(e\Phi_{12})^2 - \Delta^2 \sin^2 \theta}{\sqrt{(e\Phi_{12})^2 - \Delta^2}}. \quad (11)$$

This integral depends only on the modulus of \mathbf{q} , but not on its direction. In Eq.(11), we denote $\tilde{\omega} = \omega + e\Phi_{12}$, the limits of integration on ω are given by $\omega_1 = e\Phi_{12} + \mu_2$, $\omega_2 = \mu_1$, and the limits of integration on θ are

$$\theta_i = \begin{cases} \pi/2, & x_i > 1 \\ \sin^{-1}(x_i), & -1 < x_i < 1 \\ -\pi/2, & x_i < -1 \end{cases}, \quad x_{1,2} = \frac{2\mu_{1,2} \pm e\Phi_{12}}{\Delta}. \quad (12)$$

In obtaining Eq.(11), we parametrized \mathbf{k} -space using elliptical coordinates $k_x = k_r \sin(\theta)/2$ and $k_y = \sqrt{k_r^2 - q^2} \cos(\theta)/2$. The integration over k_r absorbs the first delta function, setting $k_r = e\Phi_{12}/\hbar v_F$, while integration over ω absorbs the second delta function fixing the limits of integration $\theta_{1,2}$ in Eq.(12). Importantly, because $\Phi_{12} > \Delta$, the two delta functions in Eq.(11) can only be satisfied simultaneously if $s = -$ and $s' = +$ (i.e. holes of

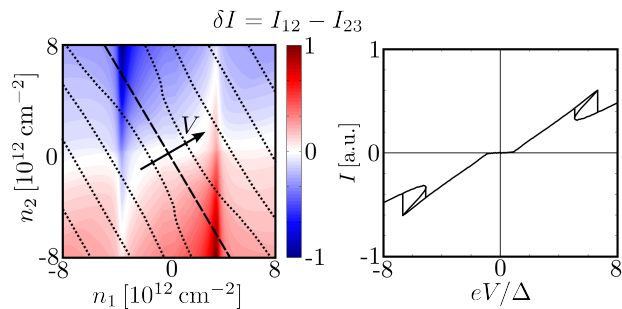


FIG. 3. Self-consistent solution obtained from Eqs.(14)–(15). Here we take n_1 and n_2 as independent parameters and calculate the current difference $\delta I = I_{12} - I_{23}$. The bias isolines from Eq.(15) are marked with dashed ($V = 0$) and dotted (finite V) lines, with an arrow pointing towards increasing V . The self-consistent $I - V$ curve, obtained from the intersection of $\delta I = 0$ and the V -isolines, is plotted in the right panel.

layer 1 tunnel into electronic states of layer 2, see Fig.2). In the scenario considered in the main text, $\mu_{1,2} = 0$ and $V_{12} = \Phi_{12}$, Eqs.(11) and (12) result in Eq.(9).

For the case $e\Phi_{12} = \Delta$, it is necessary to restore the finite linewidth to the Lorentzian spectral function $A_{i,s}(\mathbf{k}, \omega) = 2\Gamma / [(\omega - s\hbar v_F|\mathbf{k}|)^2 + \Gamma^2]$. Then, the integral for the tunneling current yields

$$\begin{aligned} & \sum_{ss'} \int \frac{d\mathbf{k}}{(2\pi)^2} \int_{\Phi_{12} + \mu_2}^{\mu_1} \frac{d\omega}{2\pi} A_{1,s}(\mathbf{k}, \omega) A_{2,s'}(\mathbf{k} + \mathbf{q}, \omega) = \\ & = \frac{2}{(\hbar v_F)^2 \sqrt{\Gamma \Delta}} \left[\int_{\mu_2}^{\Delta + \mu_1} d\omega |\omega(\omega - \Delta)|^{1/2} + \mathcal{O}(\Gamma/\Delta) \right]. \end{aligned} \quad (13)$$

In obtaining Eq.(13), we transformed the integral of the spectral functions into a dimensionless integral of the form $I_{\text{res}}(\epsilon) = \int d^2\mathbf{x} \{ [f(\mathbf{x})^2 + \epsilon] [g(\mathbf{x})^2 + \epsilon] \}^{-1}$, with $f(0) = g(0) = 0$ and a null Jacobian $\det[\partial_{\mathbf{x}}f, \partial_{\mathbf{x}}g](0) = 0$ (here $\epsilon = \Gamma/\Delta$). The dimensionless integral $I_{\text{res}}(\epsilon)$ can be shown to diverge as $I_{\text{res}} \propto \epsilon^{-1/2}$, and an expansion to leading order in powers of ϵ gives Eq.(13). Using Eq.(13) and setting $\mu_{1,2} = 0$, the peak current I_{max} in Eq.(10) of the main text is obtained.

Capacitance Effects

In the main text, we fixed the Fermi energy μ_i of the different graphene layers, independently of the applied bias. However, a more detailed and accurate model of the $I - V$ response should include the effect of the quantum capacitance, such that the graphene doping varies with V . Although the features of bistability are not significantly modified in this way, as shown below, each bistable state (for a fixed V) will be characterized by different doping values. These different doping configurations, which can be probed by in-plane transport measurements, will be a

smoking gun of the presence of intrinsic bistability. These electrostatic considerations will be discussed next.

To include capacitance effects, we note that the equilibrium condition in Eq.(7) has to be complemented with further electrostatic equations. A key insight is that the system is fully characterized once the carrier densities of each layer, n_1 , n_2 and n_3 , are known. From these values of n_i , the electrostatic potentials Φ_i , the interlayer bias potentials V_{ij} , and the Fermi levels μ_i can be found, as shown next. First, if we assume that there is no external gate, the neutrality condition relates the charge densities in the different regions of the device as

$$n_1 + n_2 + n_3 = 0. \quad (14)$$

Furthermore, the application of an external bias potential V fixes the Fermi level difference between layer 1 and layer 3 as

$$eV = \mu_1 - \mu_3 + \frac{4\pi e^2}{\kappa} (n_1 d_{13} + n_2 d_{23}). \quad (15)$$

Here d_{ij} is the interlayer distance between layer i and layer j , κ is the dielectric constant of the barrier material, and $\mu_i = \text{sign}(n_i) \hbar v_F \sqrt{\pi n_i}$. In Eq.(15), we implicitly assume that all layers are undoped at $V = 0$. Equations (7),(14), and (15) then form a closed set of equations from which n_1 , n_2 and n_3 can be determined. The remaining variables, V_{ij} and Φ_i , are functions of n_i . In particular, the electrostatic potentials are $\Phi_1 = 0$ (i.e. layer 1 is chosen as the reference layer), $\Phi_2 = -4\pi e^2 d_{12} n_1 / \kappa$, $\Phi_3 = 4\pi e^2 (n_1 d_{13} + n_2 d_{23}) / \kappa$. Additionally, the interlayer bias potentials are $V_{12} = (\mu_1 + \Phi_1) - (\mu_2 + \Phi_2)$, and $V_{23} = (\mu_2 + \Phi_2) - (\mu_3 + \Phi_3)$.

As parameters of the electrostatic model, we consider a thin device separated by dielectric barriers of thickness $d_{12} = d_{23} = 1.4 \text{ nm}$ (e.g. 4 layers of hBN), with dielectric constant $\kappa = 5$. The procedure to solve self-consistently the $I - V$ response is shown in Fig.3(a). Here, we take n_1 and n_2 as independent variables [n_3 is obtained from Eq.(14)], and we evaluate $\delta I = I_{12} - I_{23}$ in Eq.(5) (color map). For fixed V , indicated with dotted isolines in Fig.3(a), the self-consistent solutions to the equilibrium equations are given by the pair (n_1, n_2) such that $\delta I = 0$.

The resulting $I - V$ response is shown in Fig.3(b). Importantly, the $I - V$ characteristics are qualitatively the same as those found in the main text by neglecting quantum capacitance effects. Furthermore, by inspection of the n_1 and n_2 axes in Fig.3(a), we see that the difference in carrier concentration δn between each bistable state is on the order of $\delta n \sim 10^{12} \text{ cm}^{-2}$, similar to the rough estimation in the main text. These carrier concentration differences can easily be detected by lateral transport measurements and act as clear fingerprints of intrinsic bistability.